IWEX: A New Ultrasonic Array Technology for Direct Imaging of Subsurface Defects

Khalid CHOUGRANI[1], Niels PÖRTZGEN[2]

[1]Applus RTD, NDTI Technological Center
Rotterdam, The Netherlands, Tel: +31 10 2088 146, Fax: +31 10 415 80 22
E-mail: khalid.chougrani@applusrtd.com
[2]Applus RTD Project Services
Houston, TX, USA, Tel: +1 832 295 5020, Fax: +1 832 295 5001
E-mail: niels.portzgen@applusrtd.ca

Abstract

Both in new construction and in service, detection, sizing and characterization of defects are essential for integrity assessment of metal components and welds. Ultrasonic Non Destructive Inspection (NDI) using Pulse Echo (PE) technique or Time of Flight Diffraction (ToFD) have been proven to be reliable approaches to assess weld integrity. However, quantitative defect characterization with PE remains challenging because the signal caused by the reflection at the defect is very dependent on defect orientation. ToFD has sizing capabilities, but only limited capabilities in flaw characterization. In phased arrays inspection, the image obtained from sectorial scans can not be directly related to defect size and orientation. Data display and interpretation are not straightforward and require operator skills and experience. A better and more reliable ultrasonic inspection would be achieved if a methodology would be used that allows direct imaging of defects.

In this paper, we present the principles of imaging with 2D Inverse Wave Field Extrapolation (IWEX) as used in seismic exploration. The physical basis of this new imaging process is the Rayleigh II integral for back propagation which gives the possibility to extrapolate a wave field from known values at a certain surface to any location in space. The paper discusses this in detail.

The potential of IWEX for ultrasonic testing of steel components is demonstrated by several examples by which 2D and 3D images of embedded and surface defects were made. We demonstrate that location, shape, orientation and height of the defect are imaged. The interpretation of the results is straightforward, making the use of reference blocks superfluous.

Keywords: non destructive inspection, ultrasonic testing, ultrasonic imaging, detection and sizing.

1. Introduction

Detection, sizing and characterization of defects in new constructed or in service metal components are essential for its quality assessment. Many Non Destructive Inspection (NDI) methods and techniques have been developed for this purpose [1]. Ultrasonic techniques like Pulse Echo (PE) and Time of Flight Diffraction (ToFD) have been proven to be reliable detection techniques. Up to a certain extent, these techniques can also be used for sizing of defects and characterization of the defect's nature (i.e. porosity, lack of fusion or incomplete penetration). However, data obtained from these standard techniques must be interpreted and evaluated. The interpretation process is not always straightforward and can lead to inaccurate sizing of defects and hence and misjudgment of the steel component. The main reason for this is that the current sizing techniques are based on the comparison between responses from defects and responses from artificial reflectors used as a reference. As a result, large deviations may occur if these reflectors do not represent the defect sufficiently, e.g. oriented defects.

Developments have been made to improve the shortcomings of standard ultrasonic inspection techniques. Advances in computer technology and piezoelectric materials have led to new possibilities for ultrasonic inspection of steel components. An important example is the introduction of ultrasonic phased array (PA) technology for this application field. Earlier, this technology was introduced in the medical application field where it had already proven its value [2], [3], [4].

Although the beforehand mentioned techniques are widely used in NDI for both detection and sizing, it is still difficult to accurately characterize and size defects. To improve the sizing

methodology, more advanced techniques are needed. In this paper the IWEX approach will be presented whereby 2D and 3D imaging of defects become feasible.

2. The IWEX Imaging Approach

In seismic exploration, images of the subsurface are obtained from measurements of propagated waves generated by any source like vibrating trucks of explosives. The images are reconstructed using Inverse Wave Field Extrapolation (IWEX) approach [5], [6]. In this approach, the wave field recordings are extrapolated back into space towards all points in the area under investigation. If at one of those points a scatterer is present, the backwards extrapolated wave field has a high amplitude and it will give a high contribution to that location in the image. If this is done for all points in the image, the location and shape of the scatterer can be determined.

Similar to seismic applications, data recorded by ultrasonic arrays can be processed using the same imaging process. The imaging theory behind this approach is based on the Rayleigh II integral which is given in the general form by [6], [7]

$$P(\vec{r}_A,\omega)=\frac{z_A-z_0}{2\pi}\int_{-\infty}^{\infty}\int_{-\infty}^{\infty}P(\vec{r},\omega)\frac{1-j\frac{\omega}{c}\Delta r}{\Delta r^3}e^{j\frac{\omega}{c}\Delta r}dxdy \tag{1}$$

where $P(\vec{r}_A,\omega)$ is the Fourier transformed pressure in an image point A located at position $\vec{r}_A$, ω is the angular frequency and c is the medium sound velocity. $P(\vec{r},\omega)$ is the pressure recorded at z_0 and $\Delta r=\sqrt{(x-x_A)^2+(y-y_A)^2+(z_0-z_A)^2}$. Using equation (1), a recorded wave field can be extrapolated back to an arbitrary point in a 3D space from recordings over an infinite surface area. To illustrate the principle of the approach, we will continue with the 2D version and far field approximation of equation (1), which is can be written as [8], [9]

$$P(\vec{r}_A,\omega)\approx\sqrt{\frac{-j\omega}{2\pi}}\frac{z_A}{\sqrt{c}}\int_{-\infty}^{+\infty}P(x,z_0,\omega)\frac{1}{\sqrt{\Delta r}\Delta r}e^{i\omega\frac{\Delta r}{c}dx}. \tag{2}$$

This equation yields integration over an infinite recordings and over an infinite long line of receivers. However, in practice we have a limited number of receivers distributed over a limited aperture. In fact, the number of elements on the ultrasonic array and their size determine the number of receivers and the aperture length. Because of these limitations in practice, the integral of equation (2) can be written as a discrete summation over a limited number of receivers. Thus, equation (2) yields for the first step in the imaging process

$$P(n_s,0,x_A,z_A,\omega)=\sqrt{\frac{-j\omega}{2\pi}}\frac{z_A}{\sqrt{c}}\sum_{n_R}P(n_R,n_s,\omega)\frac{e^{j\omega\frac{\Delta r_{AR}}{c}}}{\Delta r_{AR}^{3/2}}\Delta x, \tag{3}$$

where n_s and n_r are the source and the receiver element numbers respectively, c the longitudinal or the transversal sound velocity, $P(n_R,n_s,w)$ are the Fourier transformed pressure recordings of source element number n_s and Δx is the center to center distance of the array elements. Note that for ultrasonic arrays, the elements can be used as source and receiver, simultaneously. With this first step, we have compensated the propagation effects from point *A* to all the receivers of a wave field generated by source element n_s.

For the second step of the imaging process, the propagation effects from the sources to point *A* should also be compensated. This can be done in a similar way and involves a summation over the number of source elements, hence

$$P(x_A,z_A,x_A,z_A,\omega)=\frac{-j\omega}{2\pi}\frac{z_A^2}{c}\sum_{n_R}\sum_{n_s}P(n_R,n_s,\omega)\frac{e^{j\omega\left(\frac{\Delta r_{AR}}{c}+\frac{\Delta r_{SA}}{c}\right)}}{\Delta r_{AR}^{3/2}\Delta r_{SA}^{3/2}}\Delta x^2. \tag{4}$$

After the second step, an amplitude will be present at $t=0$, in case a scatterer was present at location *A*. Therefore, we can assign this amplitude value to the coordinates of point *A*.

The third step of the imaging corresponds to calculate the imaging amplitude $I(x_A,z_A)$ which can be deduced by selecting the amplitude $P(x_A,z_A,x_A,z_A,t=0)$. This can be done by integration over

the frequency components. In practice the integration becomes a summation over the discrete frequency components ω_k . Consequently the final expression of the imaging amplitude becomes

$$I(x_A, z_A) = \frac{-j\omega_k}{2\pi} \frac{z_A^2}{c} \sum_{\omega_k} \sum_{n_R} \sum_{n_s} P(n_R, n_s, \omega) \frac{e^{j\omega\left(\frac{\Delta r_{AR}}{c} + \frac{\Delta r_{SA}}{c}\right)}}{\Delta r_{AR}^{3/2} \Delta r_{SA}^{3/2}} \Delta x^2 \qquad (5)$$

Finally, equation (5) formulates the way how the 2D IWEX imaging method can be implemented. Using similar analyses, an implementation for 3D imaging can be obtained from equation (1). In the following section the EWEX algorithm will be applied on ultrasonic data so that 2D and 3D images are constructed.

3. 2D and 3D Imaging using IWEX

3.1. 2D imaging of embedded defects

To apply the IWEX algorithm as described in the previous section, ultrasonic data was collected using a 4 MHz ultrasonic array consisting of 64 elements. A 10 mm carbon steel block was used in which a 2 mm slits were machined (see Figure 1). In this example the slits represents lack of fusion defects in a weld. Three situations are given where the slit is orientated, with respect to the normal direction, under an angle of 45°, 90° and 0°, respectively [8].

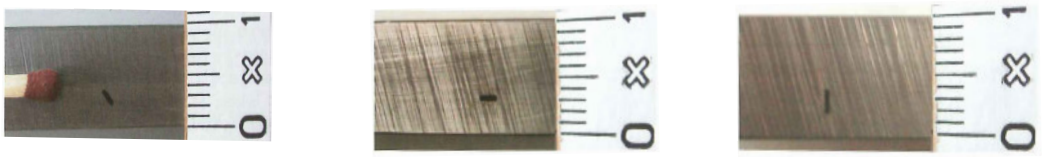

(a) (b) (c)

Figure 1: A 10 mm carbon steel block where 3 different slit orientations are illustrated (a) 45° oriented slit (b) 90° oriented slit and (c) 0° slit.

Figure 2 shows the results of the IWEX algorithm applied on the data collected by the insonification of the oriented slits 45°, 90° and 0°, respectively. The data was obtained by placing the ultrasonic array probe directly above the steel block, while a single element was used as source and all other receivers recorded the data simultaneously. This was repeated for all elements as a source, hence 64x64 A-scans were obtained for a single image.

The IWEX image can be directly compared to the original cross section as illustrated in Figure 2. It can be seen that, the location of the slit is imaged while the area directly below the slit is shadowed. Obviously, the orientation and the length of the slit are recognizable. However, the quality of the processed image depends on how the slit is oriented. For instance, the slit under an angle of 90° is optimal for direct and almost perpendicular insonification while the 0° slit orientation is less favorable. The quality dependence on the orientation is partially caused by the limited aperture and the discretization of the integral in equation (2).

Clearly, interpretation of these images is straightforward since the size, orientation and the position of the slit are visible. This suggests that data analysis using IWEX images does not require high ultrasonic skills or experience.

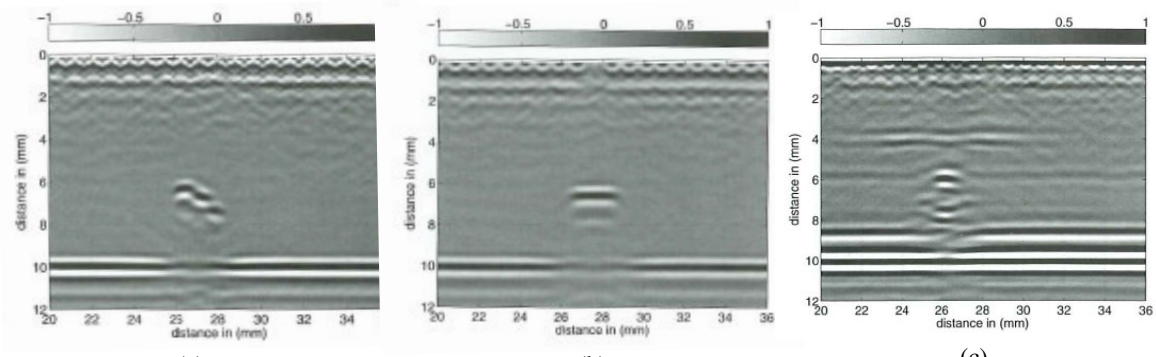

(a) (b) (c)

Figure 2: IWEX images of the 2 mm slit: (a) 45° oriented slit, (b) 90° slit orientated and (c) 0° slit oriented.

3.2. 3D imaging of an inclined slit

Following the same procedure as described in section 2, the Rayleigh II integral given in equation (1) can be applied for 3D imaging purposes. The experimental set-up used for 3D imaging is shown in Figure 3. In these experiments, a 5 MHz linear phased array with 64 elements was used. For 3D imaging, it is required that the directivity of the elements is similar to a point source, to ensure omni-directional insonification. The pitch of this array is 0.85 mm and the length of the elements is 1.9 mm. The test piece was a 25 mm thick carbon steel block which contains a 10 mm wide slit, inclined under angle of 45°.

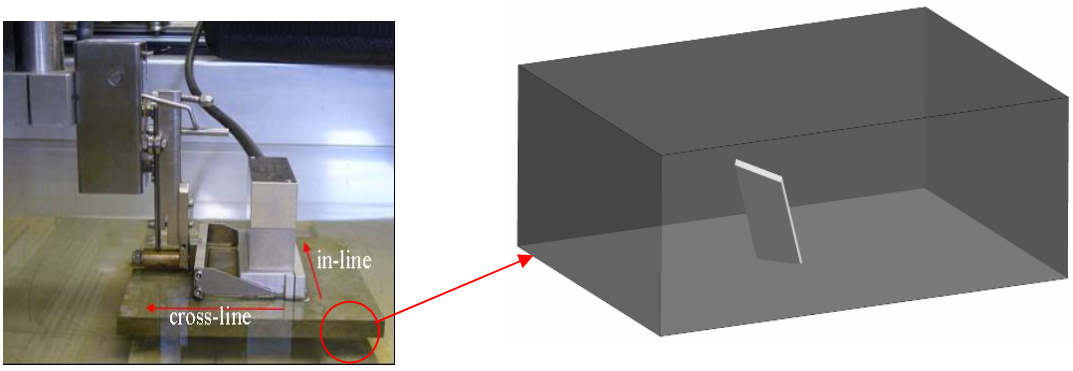

(a) (b)

Figure 3: (a) Measurement set-up, consisting of a spring loaded arm fixed to an x-y table. An ultrasonic linear array probe is mounted on the arm. The test piece (steel block) was placed in a water tank to ensure ultrasonic coupling. (b) Test piece with an inclined slit with an oblique tip.

To fully visualize the slit, a set of measurements was performed in the in-line and cross-line directions, respectively. Figure 4 represents three different views of the scatter plot that was obtained by combining and cascading both set of measurements. It can be seen that

- The flank of the slit is visible and it is inclined with respect to the back wall (Figure 4a);
- The end of the slit is visualized and skewed (Figure 4b and 4c);
- A shadow area can be seen, which is caused by the shadow effect of the slit.

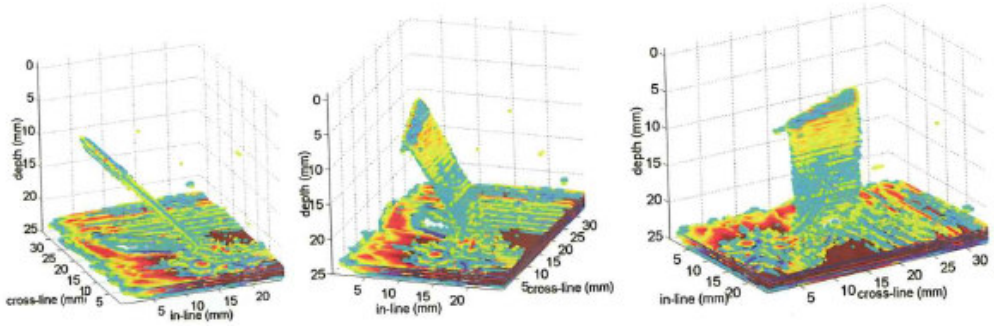

(a) (b) (c)

Figure 4: Three different views of the volumetric scatter plot. The orientation of the slit is visible of various angles.

To determine the exact inclination angle, slices through the image volume and that coincides with the flank were taken. The corresponding results are presented in Figure 5.

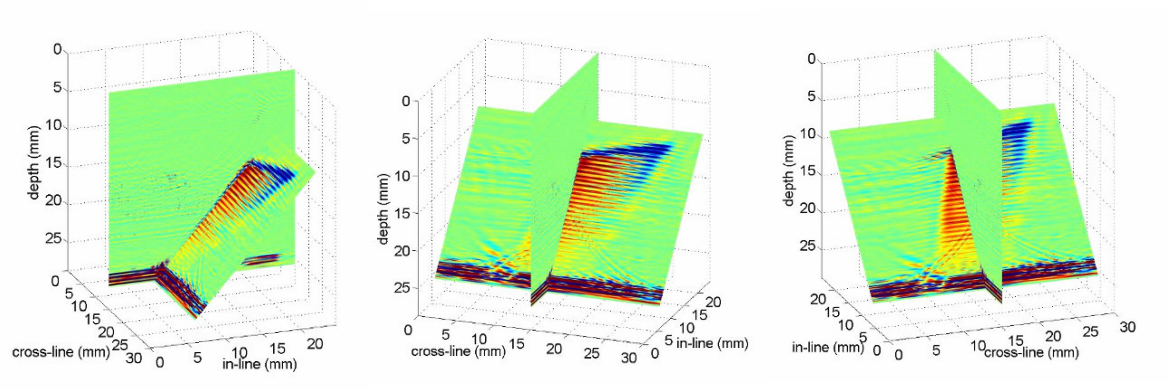

(a) (b) (c)

Figure 5: Three different views of the image volume with two slices. One of the slices coincides with the flank of the slit. In that slice the shape of the slit is clearly recognizable.

The following can be observed:

- The flank of the slit is clearly visible. It can be seen that the slit is inclined with respect to the back wall. From the inclined slice, the angle of the slit can be determined;
- It can be seen that the end of the slit is skewed. However, it remains difficult to obtain the act angle of the skewed slit end;

The amplitude of the imaged flank becomes weaker for deeper positions. This is a result of the fact that less elements can detect the deeper areas in the zero-offset configuration.

4. Conclusions

In this paper The IWEX approach has been presented. It has been shown that the ultrasonic data can be processed and constructed to visualize defects as 2D and 3D images. The imaging theory is based on the Rayleigh II integral and has been already applied in seismic applications.

The major benefit of IWEX algorithm is detection, characterization and sizing of defects without using calibration blocks. Furthermore data interpretation does not depend on the operator skills since the IWEX image is can be directly linked to the test piece under consideration.

The IWEX algorithm is not yet introduced in the operational NDI. This is due the huge amount of data needed to generate 2D and 3D images. Furthermore, data collection is time consuming and strongly depends on the current speed of computers. However, enhancement in computer technology will lead to a fast implementation in the future of the IWEX imaging in real time inspection.

References

[1] J. Krautkrämer et al, Ultrasonic Testing of Materials, Second Edition, Springer-Verlag Berlin Heidelberg New York 1977.

[2] A. Fenster et al, Three-dimensional ultrasound imaging, Physics in Medicine and Biology, volume 46, May 2001, P67-99.

[3] S. Hughes, Medical ultrasound imaging, Medical Physics, Physics Education 36, November 2001, IOP publishing Ltd. P468-475.

[4] N.T Wells, Current status and future technical advances of ultrasonic imaging, Engineering in Medicine and Biology Magazine IEEE, volume 19, September/October 2000, P14-20.

[5] A.J. Berkhout, Seismic migration imaging of acoustic energy by wave field extrapolation, Elsevier second edition, Amsterdam 1982.

[6] J.F. Claerbout, Imaging the earth's interior, Blackwell Scientific Publications (1985)

[7] N. Pörtzgen, Imaging of Defects in Girth Welds using Inverse Wave Field Extrapolation of Ultrasonic Data, Delft 2007.

[8] N. Pörtzgen et al, Inverse Wave Field Extrapolation: A different NDI Approach to Imaging Defects, IEEE transactions on UFFC, volume 54, Number 1 2007, P118-127.

[9] A.J. Berkhout, Applied seismic wave theory, Elsevier Amsterdam, Oxford, New York, Tokyo, 1987.